NANO LETTERS

2005
Vol. 5, No. 2
373−377

Synthesis of Nearly Monodisperse Embedded Nanoparticles by Separating Nucleation and Growth in Ion Implantation

Vidya Ramaswamy,[†] Tony E. Haynes,[‡] C. Woody White,[‡] Warren J. MoberlyChan,[§] Sjoerd Roorda,[||] and Michael J. Aziz*,[†]

Division of Engineering and Applied Sciences, Harvard University, Cambridge, Massachusetts, Condensed Matter Sciences Division, Oak Ridge National Laboratory, Oak Ridge, Tennessee, Center for Imaging and Mesoscale Structures, Harvard University, Cambridge, Massachusetts, and Département de physique, Université de Montréal, Montréal, QC, Canada

Received November 20, 2004; Revised Manuscript Received January 3, 2005

ABSTRACT

We investigate the formation of nanoparticles of Au in SiO_2 by multiple ion implantation steps and intermediate anneals to isolate nucleation and growth, thereby producing a narrow particle size distribution. We discuss the effects of varying the initial nucleation dose and the growth temperature and establish guidelines for synthesizing nanoparticles with improved size uniformity. By this method, we have obtained a standard deviation of 16% on an average diameter of 1.68 nm, compared to 28% when no attempt is made to isolate nucleation and growth.

Nanoparticles with novel optoelectronic[1−3] and magnetic[4] properties can be synthesized by ion implantation of one or more low-solubility species into a suitable matrix, accompanied or followed by thermal annealing.[5] The formation of nanoparticles by ion implantation has the benefit of seamless integration with wafer fabrication lines. However, the process of uncontrolled nucleation and growth by which the particles form naturally results in a broad particle size distribution, posing a limitation because the properties of the nanoparticles are often size dependent. Examples of particle size dependent properties include the metal-to-insulator transition temperature of VO_2 nanoparticles[2] and the frequency of light emission from Si nanoparticles.[3,6] In the case of Si nanoparticles in Er-doped SiO_2 for IR emission, the transfer of energy from the nanoparticles to the Er atoms may be optimal for a specific particle diameter.[7]

Chemical synthesis techniques have been used successfully to produce nearly monodisperse nanoparticles, by the temporal separation of the nucleation and growth processes.[8] Such methods, however, are not fully compatible with current wafer fabrication technology. In this paper we present a multistep processing method for controlling the size and size distribution of embedded nanoparticles formed by ion implantation: a low "nucleation" dose is implanted at room temperature, followed by a short, high temperature "spike" anneal to bring nucleation to completion; subsequently, an additional "growth" dose is implanted at an elevated temperature (lower than the spike anneal temperature), T_{growth}, under conditions chosen to minimize further nucleation. The two-step implanted samples are compared to samples in which a similar net dose was implanted in a single step at T_{growth}. Au in amorphous SiO_2 was chosen as a model system due to the inert nature of Au, its low solubility in SiO_2, and for ease of detection and measurement of small particles. The principles developed are broadly applicable to a wide range of materials systems and nanoparticles synthesis techniques. Other approaches for reducing the size distribution are also noteworthy.[9−11]

We implanted 75 keV Au^- ions into 100 nm thick thermal SiO_2 on Si substrates. For this energy, an average implant depth of 36 nm and a full width at half-maximum of 14 nm for the as-implanted Au concentration profile is predicted by SRIM[12] and was verified by Rutherford backscattering spectrometry (RBS). The ion flux was approximately 0.1 μA/cm^2. Test samples were first implanted at room temperature with a low dose of Au, ranging from 1×10^{14}/cm^2 to 5×10^{14}/cm^2. The samples were then spike annealed for 5 min at 1100 °C in an Ar-4%H_2 atmosphere. Due to the low

* Corresponding author. E-mail: maziz at harvard dot edu.
[†] Division of Engineering and Applied Sciences, Harvard University.
[‡] Oak Ridge National Laboratory.
[§] Center for Imaging and Mesoscale Structures, Harvard University.
[||] Université de Montréal.

10.1021/nl048077z CCC: $30.25
Published on Web 01/20/2005

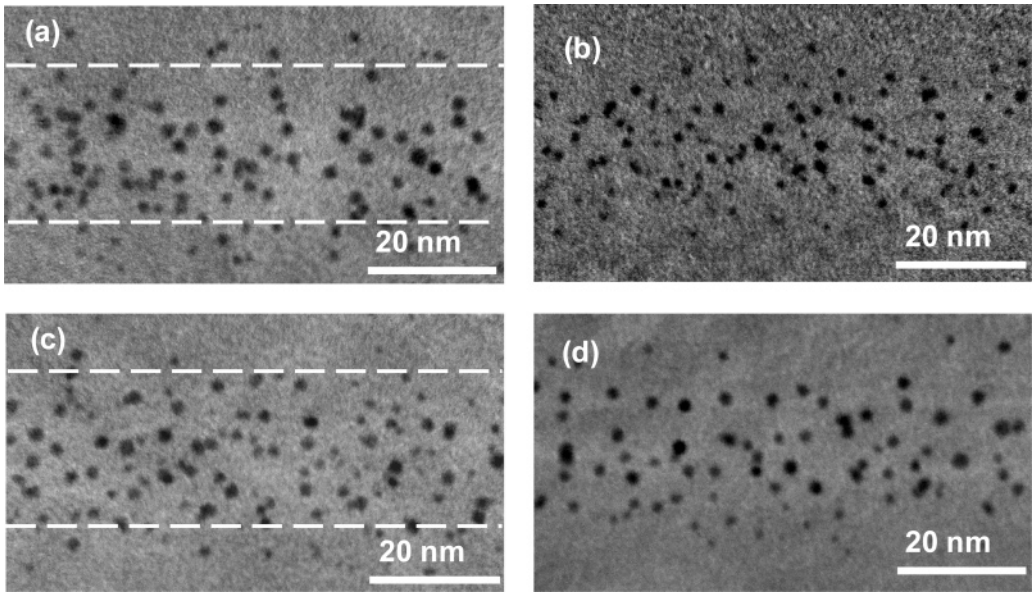

Figure 1. XTEM images for (a) 2×10^{14} at RT + spike anneal + 1×10^{15} at 700 °C; (b) 1.2×10^{15} at 700 °C; (c) 2×10^{14} at RT + spike anneal $+1 \times 10^{15}$ at 500 °C; (d) 1.5×10^{15} at 500 °C. Dashed lines in (a) and (c) mark the boundaries within which nanoparticles nucleated during the spike anneal (before the growth dose).

solubility of Au in SiO_2 a high density of Au particles nucleates, but the short annealing time and low dose do not permit significant growth or ripening. Thereafter, the samples were implanted at a high temperature, T_{growth}, with an additional growth dose of $1 \times 10^{15}/cm^2$. T_{growth} was varied from 500 °C to 700 °C, with the objective of finding conditions under which the Au added in the growth step causes only the growth of particles nucleated during the spike anneal, and no additional nucleation. For each T_{growth}, control samples were implanted in a single step with a total dose similar to the test samples. The peak concentration for a dose of $1 \times 10^{15}/cm^2$ is approximately 6×10^{20} atoms/cm^3. The average size, size distribution, and spatial distribution of Au nanoparticles in the test and control samples were obtained from cross-section transmission electron microscopy (XTEM) analyses. Samples implanted with only the nucleation dose and spike annealed were also examined by XTEM. The concentration threshold for nucleation as a function of temperature was estimated by in situ high-temperature XTEM observation of precipitation in samples implanted with a low Au dose at room temperature.

The XTEM image of a test sample with a nucleation dose of $2 \times 10^{14}/cm^2$ and a growth dose of $1 \times 10^{15}/cm^2$ implanted at $T_{growth} = 700$ °C is shown in Figure 1a, and Figure 1b is the corresponding control sample ($1.2 \times 10^{15}/cm^2$ implanted at 700 °C). Similarly, Figures 1c and 1d are micrographs of test (nucleation dose of $2 \times 10^{14}/cm^2$ and growth dose of $1 \times 10^{15}/cm^2$) and control (total dose of $1.5 \times 10^{15}/cm^2$) samples with $T_{growth} = 500$ °C. The dashed lines in Figures 1a and 1c indicate the edges of the band within which nanoparticles are observed following the nucleation dose and spike anneal without a growth dose (XTEM images not shown). It is likely that the particles in (a) and (c) lying outside this band nucleated during the growth step.

Nucleation is expected to take place during the growth step if the background concentration of Au exceeds a temperature-dependent threshold value, as indicated in Figure 2. The width of the precipitate band formed upon annealing a low dose sample can be mapped onto the implant profile, yielding a concentration threshold for perceptible nucleation under the experimental annealing conditions. The nucleation threshold concentration estimated in this manner is plotted in Figure 2 (solid triangles) for temperatures ranging from 500 °C to 1100 °C. Up to a temperature of about 800 °C, the nucleation threshold concentration decreases as the temperature is increased, indicating that in this temperature regime, nucleation is mobility-controlled. Above 800 °C, the nucleation threshold increases with increasing temperature consistent with a temperature regime in which nucleation is solubility-controlled.

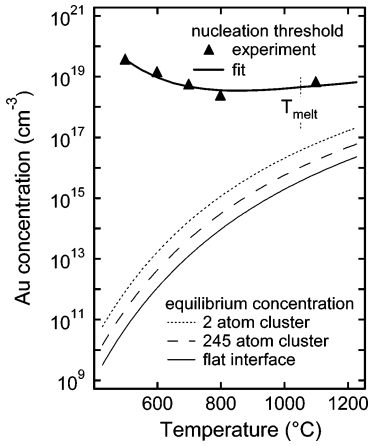

Figure 2. Temperature dependence of the concentration threshold for nucleation. Experimental data (solid triangles) was obtained from TEM heating experiments on low dose, room-temperature implanted samples. The solid line is best fit of eq 2 to the data. Also shown are the equilibrium concentrations of Au in SiO_2 for a flat interface and curved interfaces with radii of curvature corresponding to 2-atom and 245-atom (10 nm) clusters.

The nucleation rate per unit volume at temperature T from supersaturated solution with Au concentration c is given by[13]

$$I = \frac{c^2 s \nu_0}{c_{SiO_2} n^*} \left(\frac{\Delta G^*}{3\pi kT}\right)^{(1/2)} \exp\left(\frac{-\Delta G^*}{kT}\right) \exp\left(\frac{-Q}{kT}\right) \qquad (1)$$

where ΔG^* is the thermodynamic barrier to nucleation, Q is the activation barrier to diffusion, n^* is the number of atoms in a critical nucleus, and s is the number of attachment sites on a critical nucleus; the atomic density of SiO_2 is c_{SiO_2}, the atomic vibration frequency ν_0 is $\sim 10^{13}$ Hz, and k is Boltzmann's constant. For a spherical nucleus, $\Delta G^* = 16\pi\gamma^3/3(\Delta g_v)^2$, where γ is the interfacial free energy of the Au−SiO_2 interface and Δg_v is the bulk free energy change per unit volume. Setting the nucleation rate equal to its smallest discernible value I_{min}, which we estimate to be 10^{15}/(cm^{3}s), we rearrange eq 1 to obtain an expression for the threshold concentration for discernible nucleation

$$c_{nuc} = \left[\frac{n^* c_{SiO_2} I_{min}}{s\nu_0 \left(\frac{\Delta G^*}{3\pi kT}\right)^{(1/2)}}\right]^{(1/2)} \exp\left(\frac{\Delta G^*}{2kT}\right) \exp\left(\frac{Q}{2kT}\right) \qquad (2)$$

For small atomic fraction x and equilibrium value, x_{eq} (i.e., for highly immiscible systems), $\Delta g_v \approx \Omega - kT\ln x$, for $T > T_m$, and $\Delta g_v \approx \Omega - kT\ln x + \Delta g_{fusion}(T)$, for $T < T_m$, where T_m is the Au melting temperature and Ω is the regular solution parameter for the Au−SiO_2 pseudo-binary alloy. The expression for c_{nuc} (eq 2) is fit to the experimental data in Figure 2 (solid line), with fitting parameters Q and Ω, and the best fit is obtained for $Q = 1.7$ eV, in reasonable agreement with published results,[14] and $\Omega = 1.8$ eV, consistent with a large, positive enthalpy of mixing.

If noninteracting particles grow under diffusion-limited conditions, the absolute particle size distribution decreases with time.[15] Hence, if no particles nucleate during the growth step, the particle size distribution for the test samples should be narrower than that for the corresponding control samples. Precipitate size distributions corresponding to T_{growth} of 700 °C and 500 °C are plotted in Figure 3a and 3b, respectively. The average precipitate diameter (d_{avg}) of the 700 °C test sample is 1.56 nm and the standard deviation (δ) is 0.42 nm. For the 700 °C control sample, d_{avg} and δ are 1.29 and 0.36 nm, respectively. The broader absolute size distribution of the 700 °C test sample compared to the control sample suggests that new particles were nucleated during the growth step. The smaller d_{avg} of the control sample indicates a high nucleation rate during implantation, while the large d_{avg} of the test sample is due to the growth of particles formed during the spike anneal. The 500 °C control sample has $d_{avg} = 1.67$ nm and $\delta = 0.45$ nm. The 500 °C test sample has a broad, bimodal particle size distribution, with the peaks in the distribution centered roughly about 1 and 2 nm. From Figure 2, nucleation at 700 °C and 500 °C is expected to be mobility-controlled. The size distributions for the 700 °C and 500 °C control samples, in Figure 3a and 3b, respectively, are consistent with this prediction. The Au supersaturation required for discernible nucleation is higher at 500 °C than at 700 °C. Thus in the 500 °C sample, nucleation of new particles takes place late in the growth step, by which time the background supersaturation is sufficiently high; the resulting size distribution is bimodal due to the small size of these new precipitates. In contrast, at 700 °C, nucleation of new particles takes place at lower supersaturation (i.e., earlier in the growth step). Because these particles also grow by consuming the growth dose, the size distribution, although broadened, remains unimodal. Even at 500 °C, there is sufficient mobility for precipitate growth, as evidenced by the large precipitates present in the 500 °C test sample.

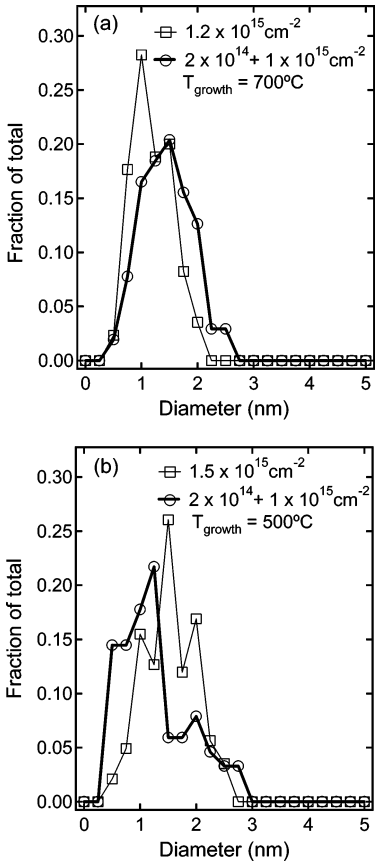

Figure 3. Size distributions for test samples (circles) and control samples (squares) with a nucleation dose of 2×10^{14}/cm^2 for (a) $T_{growth} = 700$ °C, and (b) $T_{growth} = 500$ °C.

The results above indicate that it is beneficial to keep T_{growth} low enough to remain below the nucleation threshold, while still permitting efficient precipitate growth. In the 500 °C test sample described above, precipitates with a narrow size distribution might have been obtained by decreasing the growth dose. An alternative approach is to increase the nucleation dose, thereby nucleating a higher density of precipitates during the spike anneal. At the same T_{growth}, the background supersaturation would increase more slowly during the growth dose in such a sample, due to a higher density of sinks. Figure 4a is the XTEM micrograph of a test sample with a nucleation dose of 5×10^{14}/cm^2, an 1100 °C spike anneal, and a growth dose of 1×10^{15}/cm^2, implanted at $T_{growth} = 500$ °C. Figure 4b is the corresponding control sample. The precipitate size distributions of these

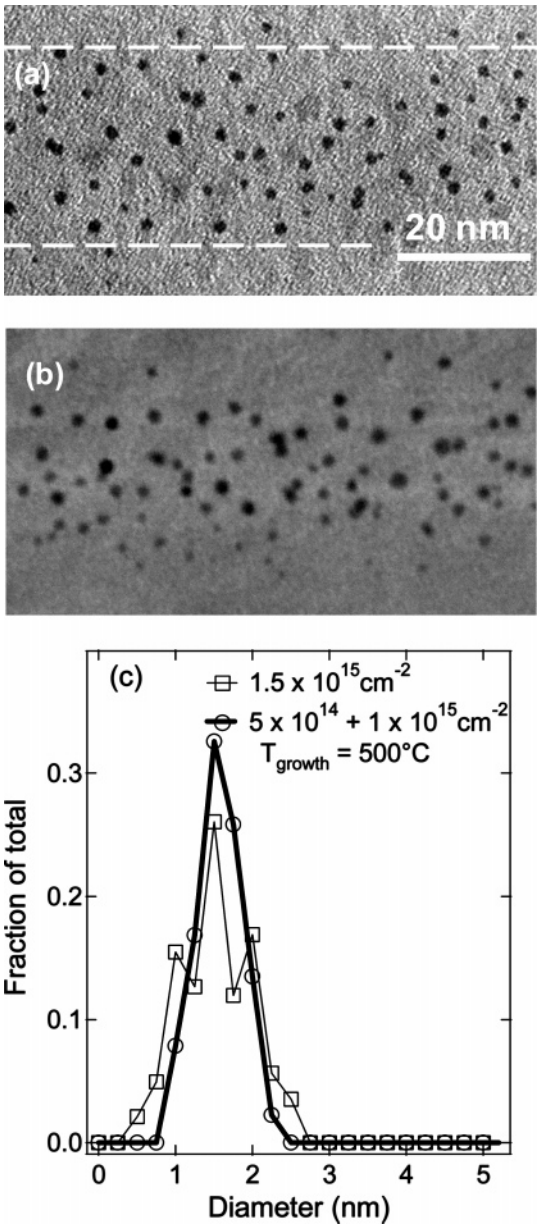

Figure 4. XTEM images of (a) 5×10^{14}/cm^3 at RT + spike anneal + 1×10^{15}/cm^3 at 500 °C and (b) 1.5×10^{15}/cm^3 at 500 °C; (c) particle size distributions corresponding to (a) and (b).

samples are compared in Figure 4c. In both samples, $d_{avg} = 1.68$ nm, but in the test sample, $\delta = 0.27$ or 16%, which is significantly narrower than $\delta = 0.47$ for the control sample. The narrowing of the particles size distribution in the test sample is not due to "inverse Ostwald ripening"[10] as this ion-stimulated process should be equally effective in both the test and control samples. We note that higher energy implantation may enhance both the diffusivity[5] and the solubility of Au in SiO_2.[11]

We have discussed the effects of nucleation during the growth step on the width of the nanoparticle size distribution. However, to obtain a narrow size distribution, in addition to preventing nucleation, it is also important to prevent Ostwald ripening of the particles. Ostwald ripening, a process by which large particles grow at the expense of smaller particles, is driven by a decrease in the total interfacial area of the system. However, small particles will not redissolve into the matrix if the solute concentration exceeds the equilibrium concentration. It is therefore useful to consider the equilibrium concentration of Au in SiO_2 as a function of nanoparticle size. The equilibrium concentration at an interface with radius R is given by the Gibbs−Thomson equation, $c_R = c_{eq}(1 + (2\gamma v/Rk_BT))$, where c_{eq} and c_R are equilibrium concentrations near a flat interface and an interface with radius of curvature R, respectively, and v is the atomic volume. The equilibrium atomic fraction adjacent to a flat interface is expressed as $x_{eq} = \exp(\Omega/kT)$. Figure 2 includes plots of c_{eq} and c_R, for R corresponding to a 2-atom cluster and a 245-atom (10-nm) cluster, as functions of T. For mean field concentration $c > c_R$, particles with radii greater than or equal to R are stable with respect to dissolution. If the smallest possible particle, i.e., a 2-atom cluster, is stable, the system is not susceptible to Ostwald ripening.[16] Hence for a given temperature, $c_R(T)$ for a 2-atom cluster represents a threshold concentration above which Ostwald ripening does not occur. In Figure 2, we can identify a $c-T$ process window within which neither nucleation of new particles nor the Ostwald ripening of existing particles occurs. In this window, existing particles will grow by draining the Au supersaturation, and the size distribution should evolve to become narrower. This concentration window is widest at lower temperatures.

Our results suggest the following strategy to control the average particle size and particle density: (a) choosing nucleation conditions to tailor the particle density, and (b) choosing conditions of the growth implant to provide enough mobility for growth while keeping the internucleus concentration below the threshold for further nucleation and above that for Ostwald ripening. In principle, in the mobility-controlled regime, this may be done by a variety of methods such as restricting the growth dose, reducing the growth flux, or alternate implant and anneal steps. In principle, the latter approach can be used to produce particles of arbitrarily large size as long as each step remains within the $c-T$ process window.[17] Ultimately, fluctuation effects not accounted for in the mean field picture will limit the sharpness of the size distribution. Some aspects of this phenomenon have been studied in the setting of 2D submonolayer island nucleation and growth in steady deposition from the vapor,[18] but we are not aware of studies of 3D systems or non−steady processes.

In summary, using Au implanted SiO_2 as a model system, we have demonstrated that separating the nucleation and growth of nanoparticles by multiple implantation steps can substantially reduce the breadth of the size distribution of nanoparticles formed by ion implantation. The strategy used was to choose a growth temperature that is low enough to inhibit nucleation but high enough to efficiently drain the background supersaturation. The present study was not a process optimization, and a further reduction in the breadth of the size distribution should be possible by refinements of this process. This approach will be useful when nanoparticles of a specific size and narrow size distribution, embedded in crystalline or amorphous matrixes, are desired. The principles

illuminated here are also applicable to other synthesis processes such as the growth of monodisperse islands by vacuum or electrodeposition.

Acknowledgment. This research was supported by NSF-DMR-0210785 and the Harvard NSEC (NSF-PHY-0117795) at Harvard University, and by the U.S. Department of Energy (contract DE-AC05-00OR22725 with UT-Battelle, LLC) at ORNL. We are thankful to D. K. Thomas (ORNL) for valuable assistance with ion implantation.

References

(1) Magruder, R. H., III; Yang, L.; Haglund, R.; White, C. W.; Yang, L.; Dorsinville, R.; Alfano, R. R. *Appl. Phys. Lett.* **1993**, *62*, 1730.
(2) Lopez, R.; Haynes, T. E.; Boatner, L. A.; Feldman, L. C.; Haglund, R. F. *Phys. Rev. B* **2002**, *65*, 224113.
(3) Skorupa, W.; Rehbohle, L.; Gebel, T. *Appl. Phys. A* **2003**, *76*, 1049.
(4) Meldrum, A.; Boatner, L. A.; White, C. W. *Nucl. Instrum. Methods B* **2001**, *178*, 7.
(5) White, C. W.; Zhou, D. S.; Budai, J. D.; Zhur, R. A.; Magruder, R. H., III; Osborne, D. H. *Mater. Res. Soc. Symp. Proc.* **1994**, *316*, 499.
(6) Guha, S.; Qadri, S. B.; Musket, R. G.; Wall, M. A.; Shimizu-Iwayama, T. *J. Appl. Phys.* **2000**, *88*, 3954.
(7) Pacifici, D.; Irrera, A.; Franzo, G.; Miritello, M.; Iacona, F.; Priolo, F.; *Physica E* **2003**, *16*, 331.
(8) Murray, C. B.; Norris, D. J.; Bawendi, M. G. *J. Am. Chem. Soc.* **1993**, *115*, 8706.
(9) Valentin, E.; Bernas, H.; Ricolleau, C.; Creuzet, F. *Phys. Rev. Lett.* **2001**, *86*, 99.
(10) Rizza, G. C.; Strobel, M.; Heinig, K.-H.; Bernas, H. *Nucl. Instrum. Methods B* **2001**, *178*, 78.
(11) Rizza, G. C.; Strobel, M.; Heinig, K.-H.; Bernas, H. *Nucl. Instrum. Methods B* **2001**, *178*, 78.
(12) Ziegler, J. F.; Biersack, J. P.; Littmark, U. *The Stopping and Range of Ions in Solids*; Pergamon Press: New York, 1985.
(13) Christian, J. W. *The Theory of Transformations in Metals and Alloys, Part I*; Pergamon Press: New York, 2002.
(14) Miotello, A.; De Marchi, G.; Mattei, G.; Mazzoldi, P.; Sada, C. *Phys. Rev. B* **2001**, *63*, 075409.
(15) Reiss, H. *J. Chem. Phys.* **1951**, *19*, 482.
(16) We note that although the capillary approximation is likely to break down for nanoparticles this small, the error is still likely to be insignificant compared to the 10 orders of magnitude spanned by the ordinate in Figure 2.
(17) Note that within the current theoretical framework, as the target nanoparticle size increases, the target nucleation density (in the nucleation step) will decrease; therefore the diffusion distance in the growth step must increase and so must the growth time or temperature. These considerations will necessitate multiple, incremental growth steps to achieve large particle sizes and may impose practical limitations on particle size.
(18) Amar, J. G.; Popescu, M. N.; Family, F. *Phys. Rev. Lett.* **2001**, *86*, 3092.

NL048077Z